J Nanopart Res (2012) 14:1175
DOI 10.1007/s11051-012-1175-z

RESEARCH PAPER

Relative binding affinity of carboxylate-, phosphonate-, and bisphosphonate-functionalized gold nanoparticles targeted to damaged bone tissue

Ryan D. Ross · Lisa E. Cole · Ryan K. Roeder

Received: 3 April 2012 / Accepted: 30 August 2012

Abstract Functionalized Au NPs have received considerable recent interest for targeting and labeling cells and tissues. Damaged bone tissue can be targeted by functionalizing Au NPs with molecules exhibiting affinity for calcium. Therefore, the relative binding affinity of Au NPs surface functionalized with either carboxylate (L-glutamic acid), phosphonate (2-aminoethylphosphonic acid), or bisphosphonate (alendronate) was investigated for targeted labeling of damaged bone tissue in vitro. Targeted labeling of damaged bone tissue was qualitatively verified by visual observation and backscattered electron microscopy, and quantitatively measured by the surface density of Au NPs using field-emission scanning electron microscopy. The surface density of functionalized Au NPs was significantly greater within damaged tissue compared to undamaged tissue for each functional group. Bisphosphonate-functionalized Au NPs exhibited a greater surface density labeling damaged tissue compared to glutamic acid- and phosphonic acid-functionalized Au NPs, which was consistent with the results of previous work comparing the binding affinity of the same functionalized Au NPs to synthetic hydroxyapatite crystals. Targeted labeling was enabled not only by the functional groups but also by the colloidal stability in solution. Functionalized Au NPs were stabilized by the presence of the functional groups, and were shown to remain well dispersed in ionic (phosphate buffered saline) and serum (fetal bovine serum) solutions for up to 1 week. Therefore, the results of this study suggest that bisphosphonate-functionalized Au NPs have potential for targeted delivery to damaged bone tissue in vitro and provide motivation for in vivo investigation.

Keywords Binding affinity · Bisphosphonate · Bone microdamage · Contrast agent · Gold nanoparticles · Targeted delivery

Electronic supplementary material The online version of this article (doi:10.1007/s11051-012-1175-z) contains supplementary material, which is available to authorized users.

R. D. Ross
Department of Anatomy and Cell Biology, Rush University Medical Center, Chicago, IL 60612, USA

R. D. Ross · L. E. Cole
Department of Aerospace and Mechanical Engineering Bioengineering Graduate Program, University of Notre Dame, 225 Multidisciplinary Research Building, Notre Dame, IN 46556, USA

R. K. Roeder (✉)
Department of Aerospace and Mechanical Engineering Bioengineering Graduate Program, University of Notre Dame, 148 Multidisciplinary Research Building, Notre Dame, IN 46556, USA
e-mail: rroeder@nd.edu

Introduction

Gold nanoparticles (Au NPs) are commonly used as a contrast agent for electron microscopy (Stirling 1990; Hermann et al. 1996), and are being investigated as a

Published online: 12 September 2012

contrast agent for X-ray imaging, due to exhibiting a high mass density, atomic number, and electron density (Hainfeld et al. 2006; Sperling et al. 2008). Au NPs have received considerable recent interest as an X-ray contrast agent due to exhibiting relatively high X-ray attenuation compared to current clinical contrast agents based on iodinated molecules, such as Omnipaque (Hainfeld et al. 2006; Xu et al. 2008), Iobrix (Cai et al. 2007), Ultravist (Kim et al. 2007), and Iopromide (Jackson et al. 2010). Au NPs have also exhibited improved vascular retention compared to iodinated contrast agents, which could extend the available time-window for clinical imaging and enhance delivery (Hainfeld et al. 2006; Cai et al. 2007; Kim et al. 2007).

Au NPs are also readily surface functionalized for colloidal stability and/or targeted delivery (Sperling et al. 2008). Initial experiments investigating Au NPs as a vascular X-ray contrast agent utilized polyethylene glycol (PEG) to provide colloidal stability and improve the blood pool half-life (Hainfeld et al. 2006). Au NPs surface functionalized with various antibodies are widely used for immunogold labeling of proteins and cellular components for electron microscopy (Stirling 1990; Hermann et al. 1996), which has been recently applied to targeting cancerous cells for detection and/or destruction (Eck et al. 2010; Hainfeld et al. 2010; Popovtzer et al. 2008).

Surface-functionalized Au NPs were recently investigated for targeting calcified tissue to label microdamage in bone tissue (Zhang et al. 2010; Ross and Roeder 2011). Microdamage (e.g., microcracks) accumulates in bone in vivo due to mechanical loading and aging, and has been implicated in clinical fracture susceptibility (Burr et al. 1997; Chapurlat and Delmas 2009). Conventional methods for imaging microdamage are inherently two-dimensional, destructive, invasive, and tedious (Lee et al. 2003). Contrast-enhanced micro-computed tomography (micro-CT) using a precipitated barium sulfate ($BaSO_4$) stain recently enabled non-destructive and three-dimensional imaging of microdamage in tissue specimens and whole bones (Wang et al. 2007; Leng et al. 2008; Landrigan et al. 2011; Turnbull et al. 2011). However, staining by $BaSO_4$ precipitation is non-specific, and the staining solutions are also not biocompatible, limiting $BaSO_4$ labeling to in vitro experiments. Therefore, glutamic acid-functionalized Au NPs were prepared and investigated for targeting microdamage via chelation of carboxylate ligands with calcium ions on mineral surfaces which are exposed in damaged or disrupted tissue (Zhang et al. 2010), similar to fluorochrome labels (e.g., calcein) which are widely used in bone histology (O'Brien et al. 2002; Lee et al. 2003; Parkesh et al. 2007).

Bisphosphonate (alendronate)-functionalized Au NPs were shown to exhibit more rapid binding kinetics and greater binding affinity to hydroxyapatite compared to carboxylate (L-glutamic acid) and phosphonate (2-aminoethylphosphonic acid) functional groups (Ross and Roeder 2011). These functional groups (Fig. 1, insets) were chosen due to a known affinity for calcium ions on apatite crystal surfaces (Ross and Roeder 2011), which are exposed due to the disruption of the protein–mineral interface upon the formation of a crack or inelastic deformation (Lee et al. 2003). The use of hydroxyapatite crystals as a synthetic bone mineral analog enabled accurate quantitative measurements of binding isotherms. However, results for binding to synthetic crystals may not reflect binding to tissue which also contains organic matter and smaller mineral crystals with a more disordered crystalline structure, leading to the motivation for this study.

Therefore, the primary aim of this study was to investigate and compare the binding affinity of Au NPs surface functionalized with either carboxylate (L-glutamic acid), phosphonate (2-aminoethylphosphonic acid), or bisphosphonate (alendronate) for targeting damaged bone tissue in vitro. Moreover, in vivo delivery also requires colloidal stability in physiological media. Therefore, a secondary aim of this study was to characterize the colloidal stability of carboxylate-, phosphonate-, or bisphosphonate-functionalized Au NPs within phosphate buffered saline (PBS) and fetal bovine serum (FBS) in vitro.

Experimental methods

Synthesis and functionalization of Au NPs

Au NPs were synthesized to a mean particle diameter of $\sim$13 nm using the citrate reduction method (Turkevich et al. 1951), as described previously (Zhang et al. 2010; Ross and Roeder 2011). In brief, 0.1 g of $HAuCl_4 \cdot 3H_2O$ ($\geq$99 %, Sigma-Aldrich, St. Louis, MO) was added to 400 mL of de-ionized (DI) water and the solution was boiled vigorously while stirring. A 1 % solution of trisodium citrate

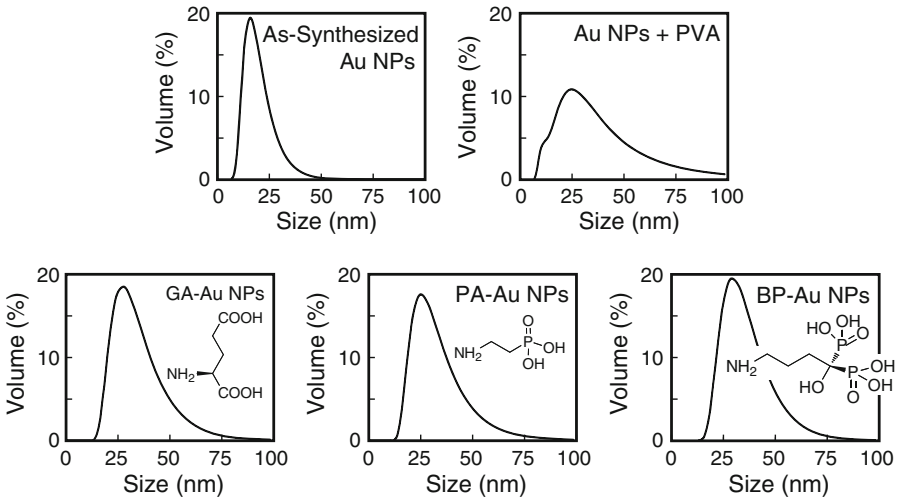

Fig. 1 Hydrodynamic particle diameter distributions measured by DLS for as-synthesized, citrate-stabilized Au NPs, PVA-stabilized Au NPs, and Au NPs surface functionalized with glutamic acid (GA), phosphonic acid (PA), or bisphosphonate (BP). The molecular structure of each functional group is shown schematically. The mean hydrodynamic diameter increased from 19 nm for as-synthesized, citrate-stabilized Au NPs to 40–50 nm for PVA-stabilized Au NPs and surface functionalized Au NPs (Table 1)

dehydrate (ACS reagent, >99.0 %, Sigma-Aldrich) was added to the boiling solution at a mass ratio of 5:1 $HAuCl_4$ to sodium citrate and left boiling for an additional 20 min. The solution volume was then adjusted to a total of 500 mL using DI water. The resulting Au NP solution had a gold concentration of ~0.5 mM and a wine red color.

Au NPs were prepared for functionalization by first removing excess citrate ions. 1.5 mL 2 % polyvinyl alcohol (PVA 10–98, 61,000 Da, Fluka, St. Louis, MO) was added to 24 mL Au NP solution, followed by 0.6 g ion exchange resin (Amberlite MB-150, Sigma-Aldrich). The resulting solution was stirred overnight and subsequently filtered (grade 3, Whatman, Piscataway, NJ) to remove spent ion exchange resin. Au NPs were surface functionalized by adding 1 mL of a 0.01 M solution of either L-glutamic acid (≥99.5 %, Fluka), 2-aminoethylphosphonic acid (99 %, Sigma-Aldrich), or alendronate sodium trihydrate (≥97 %, Sigma-Aldrich) (Fig. 1, insets). The solution was left to equilibrate overnight under mild stirring. Excess functionalization molecules were removed by dialysis (Spectra/Por, MWCO = 3,500 Da, Spectrum Laboratories, Rancho Dominguez, CA) against DI water for a total of 3 days, changing the water solution at least twice daily.

Surface functionalization of Au NPs with these molecules was previously verified by Fourier-transform infrared spectroscopy (Ross and Roeder 2011). The absorption of amines onto gold surfaces occurs due to the formation of a weak covalent bond, as well as an electrostatic complex between the positively charged amine groups and chloroaurate ions on Au NP surfaces (Leff et al. 1996; Kumar et al. 2003; Selvakannan et al. 2003; Aslam et al. 2004). The mean (±standard deviation) surface density of glutamic acid, phosphonic acid, and bisphosphonate was 5.01 (0.02), 4.96 (0.02), and 3.25 (0.14) μmol/mg Au, respectively, as measured by mass spectroscopy (Ross and Roeder 2011). The lower surface density of bisphosphonate was most likely due to steric interactions of the larger bisphosphonate molecules.

Characterization of functionalized Au NPs

All gold concentrations were verified using inductively coupled plasma-optical emission spectroscopy (ICP-OES, Optima 7000, PerkinElmer, Inc., Waltham, MA). The hydrodynamic particle diameter distribution and the mean hydrodynamic particle diameter (z-average) were measured for as-synthesized and functionalized Au NPs using dynamic light scattering (DLS, Zetasizer Nano ZS90, Malvern Instruments Ltd., Worcestershire, UK). Au NP solutions were diluted in DI water to a final gold concentration of ~50 mg/L, to prevent inaccuracies associated with

multiple scattering, and reported as the mean of three measurements. PVA was added to a solution of as-synthesized Au NPs without additional functionalization in order to determine the effect of PVA alone on the hydrodynamic particle diameter. Zeta potential (Zetasizer Nano ZS90, Malvern), pH (SensIon 4, Hach Company, Loveland, CO), and viscosity (Vibro Viscometer SV-10, A&D Co. Ltd., Japan) were also measured for Au NP solutions before and after surface functionalization without further dilution and reported as the mean of three separate measurements. The mean particle diameter, particle size distribution, and the morphology of Au NPs before and after surface functionalization were previously measured using transmission electron microscopy; Au NP surface functionalization did not affect particle size or shape (Ross and Roeder 2011).

The colloidal stability of as-synthesized and surface-functionalized Au NPs was characterized using ultraviolet–visible (UV–vis) spectroscopy (Nanodrop 2000c, Thermo Scientific, Wilmington, DE). The colloidal stability of functionalized Au NPs was also characterized by both UV–vis spectroscopy and DLS after diluting equal volumes of Au NPs and either DI water, PBS (Amresco, Solon, OH), or 10 % FBS (Omega Scientific, Tarzana, CA) in PBS, to a final gold concentration of ~40 mg/L. The surface plasmon resonance (SPR) peak and mean hydrodynamic particle diameter were measured at 0 (as-prepared), 2, and 7 days following dilution.

Labeling damaged bovine cortical bone specimens

Cortical bone specimens, 5 × 5 × 5 mm, were sectioned from the diaphysis of bovine tibiae using a diamond wafer saw (Isomet, Buehler, Lake Bluff, IL). The surface normal to the radial anatomic direction was polished to a 1 μm finish using diamond compounds and washed thoroughly with DI water. Specimens were subsequently immersed in a 5 mL solution containing 0.5 mM calcein (ICN Biomedicals Inc., Aurora, OH) for 30 min under vacuum (~50 mmHg) to label (or mask) microdamage caused by the machining and specimen preparation. In order to create damage in a repeatable and observable manner, a single scratch was created on the polished specimen surface using a scalpel blade (O'Brien et al. 2002; Parkesh et al. 2007; Zhang et al. 2010). Damaged tissue specimens were then submerged into a 5 mL solution of functionalized Au NPs at a gold concentration of ~75 mg/L for 24 h under vacuum (~50 mmHg) to label the scratch. Upon removal from Au NP solutions, specimens were thoroughly rinsed, dehydrated by soaking in 70, 80, and 90 % ethanol solutions for 2 h each, followed by 100 % ethanol for at least 8 h, and finally placed into a dessicator to dry overnight.

Two additional control groups were prepared. An imaging control specimen was prepared in the manner described above, except not labeled by Au NPs, to provide visual evidence (in addition to the spectroscopic analyses below) that spherical nanoparticles observed by electron microscopy in experimental groups were due to labeling by Au NPs and not the inherent structure of the damaged tissue. Surface roughness control specimens were also prepared in the manner described above, except damage created by the scratch was labeled (or masked) by calcein (the same as the machining damage) prior to labeling with bisphosphonate-functionalized Au NPs, to demonstrate that Au NP labeling of damaged tissue in experimental groups was targeted and not influenced by the greater surface roughness of the scratch relative to surrounding tissue. Surface roughness control specimens were labeled only by bisphosphonate-functionalized Au NPs since other functional groups exhibited lower binding affinity.

Stereomicroscopy (SMZ800, Nikon Instruments, Melville, NY) was used to show the visible color change of damaged tissue due to Au NP labeling. Specimens were subsequently coated with 1.5 nm Ir (208 HR, Cressington Scientific Instruments Ltd, Watford, UK) to decrease charging of the non-conducting bone surfaces for scanning electron microscopy (SEM). The relative contrast provided by Au NPs labeling damaged tissue inside the scratch compared to undamaged tissue outside the scratch was qualitatively characterized by SEM (Evo 50, LEO Electron Microscopy Ltd., Cambridge, UK) using backscattered electron imaging (BEI) at an accelerating voltage of 20 kV and working distance of ~6 mm. The presence of elemental gold was verified by electron probe microanalysis using energy dispersive spectroscopy (INCA x-sight model 7636, Oxford Instruments America, Concord, MA).

Quantitative measurements of the Au NP surface density were obtained by field-emission scanning electron microscopy (FE-SEM, Magellan 400 XHR,

FEI, Hillsboro, OR) using secondary electron imaging (SEI) at an accelerating voltage of 3 kV, a current of 3.1 pA, and a dwell time of 30 μs. Specimen surfaces were imaged inside and outside the damaged (scratched) region and the number of Au NPs per unit projected surface area was measured using standard stereological methods (ImageJ, NIH, Bethesda, MD). In total, three randomly selected fields of view were analyzed both inside and outside the damaged (scratched) region on five specimens per experimental (functional) group. Each field of view sampled a projected surface area of 0.25 μm^2. Differences in the Au NP surface density were compared by two-way analysis of variance (ANOVA) with a Tukey's HSD post hoc test (JMP 9.0.2, SAS Institute, Inc., Cary, NC). The level of significance was set at $p < 0.05$.

Results and discussion

Characterization of functionalized Au NP solutions

The mean hydrodynamic particle diameter measured by DLS increased from 19 nm for as-synthesized, citrate-stabilized Au NPs to 40–46 nm for functionalized Au NPs (Fig. 1; Table 1). In contrast, the physical particle diameter was previously measured by transmission electron microscopy to be ~13 nm and unchanged after surface functionalization (Ross and Roeder 2011). Recall that PVA was added to maintain colloidal stability during the removal of citrate ions prior to surface functionalization. The mean (±standard deviation) hydrodynamic diameter measured for PVA-stabilized Au NPs prior to surface functionalized was increased to 52.9 (0.5) nm (Fig. 1). This suggests that the increased hydrodynamic diameter of surface-functionalized Au NPs was due to a weak interaction of PVA molecules with soluble Au NPs. The hydrodynamic particle diameter is defined as a hard sphere approximation for a particle with an equivalent translational diffusion coefficient to the particle being measured (Podzimek 2011). Therefore, the hydrodynamic diameter accounts for both strong and weak surface interactions for both the functional groups and PVA molecules, respectively, and may be more relevant to colloidal stability and deliverability than physical particle dimensions.

The zeta potential of Au NP solutions decreased from −25 mV for as-synthesized Au NPs to −10 to −11 mV after surface functionalization (Table 1), as expected due to the displacement of highly charged, surface-adsorbed citrate molecules by the functional molecules and the interaction of PVA with functionalized Au NPs. Therefore, the mechanism of colloidal stability shifted from only electrostatic stabilization of as-synthesized Au NPs to both steric and electrostatic stabilization of functionalized Au NPs due to the adsorbed molecules and associated PVA. The mean (±standard deviation) zeta potential of PVA-stabilized Au NPs prior to surface functionalized was −32.9 (0.7) mV, most likely due to the removal of counter ions (such as Na^+, Ca^{2+}, and including free citrate but not adsorbed citrate) by ion exchange prior to surface functionalization. These results suggest that the interaction between adsorbed surface functional molecules and PVA decreased the negative charge associated with the electronegative functional groups.

The association of PVA with functionalized Au NPs was confirmed to have no influence on the hydroxyapatite binding affinity. As-synthesized, PVA-stabilized Au NPs exhibited no binding affinity for hydroxyapatite in the absence of functional groups, and the binding affinity of functionalized Au NPs prepared with (Ross and Roeder 2011) and without PVA was not different (data not shown). Moreover, the

Table 1 The mean (±standard deviation) hydrodynamic particle diameter, zeta potential, pH, and viscosity of as-synthesized Au NPs, and Au NPs surface functionalized with glutamic acid (GA), phosphonic acid (PA), and bisphosphonate (BP), dispersed in DI water

Group	Hydrodynamic diameter (nm)	Zeta potential, ζ (mV)	pH	Viscosity, μ (mPa·s)
Au NPs	19.3 (0.3)	−25.2 (1.9)	6.7 (0.4)	0.92 (0.04)
GA-Au NPs	46.4 (2.9)	−10.0 (3.6)	4.7 (0.3)	0.93 (0.14)
PA-Au NPs	40.0 (2.5)	−10.8 (2.0)	4.6 (0.4)	0.91 (0.13)
BP-Au NPs	43.5 (1.9)	−11.2 (1.8)	4.7 (0.4)	0.91 (0.09)

addition of PVA and surface functionalization had no effect on the Au NP solution viscosity (Table 1). This suggests that the PVA concentration was sufficiently low to avoid increased viscosity due to the relatively high molecular weight of PVA. The addition of acidic functional groups decreased the pH of Au NP solutions (Table 1), raising the importance of examining colloidal stability in buffering and physiological media.

Characteristic SPR peaks in UV–vis spectroscopy were observed at ~527 nm, for both as-synthesized and functionalized Au NPs. SPR peaks for functionalized Au NP solutions remained unchanged for up to 7 days in DI water, PBS, and FBS media (Fig. 2), indicating that functionalized Au NPs remained well dispersed in buffered and physiological solutions. In contrast, as-synthesized Au NPs rapidly formed visible precipitates in PBS and FBS. Therefore, surface functionalization improved the colloidal stability of Au NPs in ionic solvents and serum solutions.

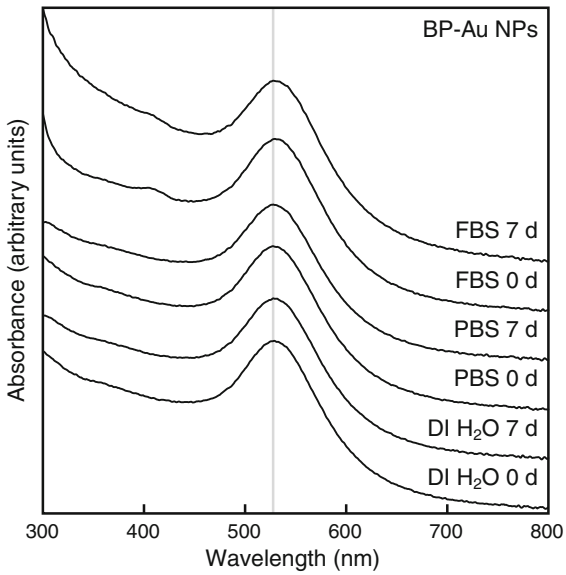

Fig. 2 UV–vis spectra for bisphosphonate (BP)-functionalized Au NPs dispersed in either DI water, PBS, or 10 % FBS solutions after 0 (as-prepared) and 7 days. The location of the SPR peak was unchanged in each media after 7 days, indicating that functionalized Au NPs remained well dispersed after dilution in physiological solutions with high ionic strength and soluble proteins. A gray reference line is shown at ~527 nm for comparison. Note that differences in the spectra at 300–350 nm for FBS were due to a peak at ~280 nm associated with serum proteins. Similar UV–vis spectra for glutamic acid (GA)- and phosphonic acid (PA)-functionalized Au NPs are available as Electronic Supplementary Material

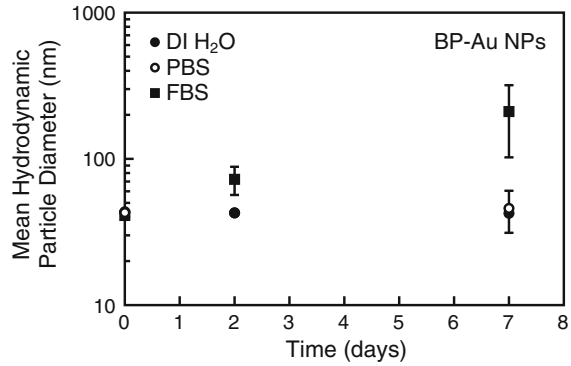

Fig. 3 The mean hydrodynamic particle diameter measured by DLS for bisphosphonate (BP)-functionalized Au NPs dispersed in either DI water, PBS, or 10 % FBS solutions after 0 (as-prepared), 2, and 7 days. Error bars show one standard deviation. The mean hydrodynamic particle diameter was unchanged in DI water and PBS for up to 7 days, but increased in FBS due to protein coagulation. Similar measurements of the mean hydrodynamic particle diameter for glutamic acid (GA)- and phosphonic acid (PA)-functionalized Au NPs are available as Electronic Supplementary Material

The mean hydrodynamic particle diameter measured by DLS for functionalized Au NPs was also unchanged for up to 7 days in water and PBS (Fig. 3), again indicating that functionalized Au NPs remained well dispersed in ionic media. In FBS, however, the mean hydrodynamic diameter increased five- to sevenfold over 7 days (Fig. 3). This increase may have occurred due to surface coating of the charged, functionalized Au NPs with soluble serum proteins, as previously reported for gold nanorods (Alkilany et al. 2009). However, considering that the SPR peaks remained unchanged, a more likely explanation was coagulation and precipitation of serum proteins themselves, which was visibly apparent. Interaction with serum proteins was previously shown to decrease the overall magnitude of the binding affinity for hydroxyapatite, but differences in the relative binding affinity between functional groups were unaffected (Ross and Roeder 2011). Thus, the improved stability of functionalized Au NPs in serum solutions suggests potential for in vivo applications, although future work must investigate stability and deliverability in vivo.

Targeted labeling of damaged bone tissue

Targeted labeling of damaged tissue in specimens was readily apparent by visual observation of the characteristic red color within scratches, which was absent in

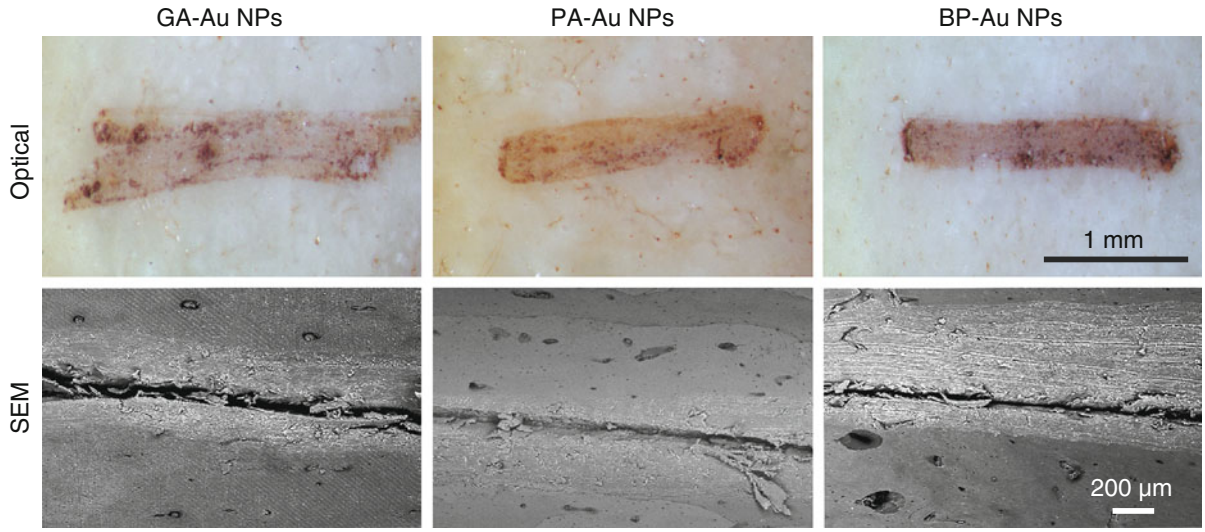

Fig. 4 Representative optical and backscattered electron micrographs showing surface damage (scratch) on bovine cortical bone specimens labeled with glutamic acid (GA)-, phosphonic acid (PA)-, and bisphosphonate (BP)-functionalized Au NPs. The relative depth of the color or contrast observed in optical and backscattered electron micrographs, respectively, for damaged bone tissue inside the scratch versus undamaged tissue outside the scratch qualitatively suggested that BP-Au NPs exhibited the greatest binding affinity for damaged bone tissue. Note that the crack along the entire length of each scratch in electron micrographs occurred upon drying the specimen for electron microscopy and was therefore not labeled by functionalized Au NPs

undamaged regions (Fig. 4). Bisphosphonate-functionalized Au NPs appeared to exhibit the greatest binding affinity by qualitative differences in the color of damaged tissue (Fig. 4). Additional evidence for targeted labeling of damaged tissue was confirmed by differences in the brightness between damaged and undamaged tissue using backscattered electron microscopy (Fig. 4). Bisphosphonate-functionalized Au NPs again appeared to exhibit the greatest binding affinity by qualitative differences in the contrast between damaged and undamaged tissue (Fig. 4). Image contrast from backscattered electrons is primarily due to compositional differences in atomic number, with an increasing atomic number resulting in increased brightness. Furthermore, the presence of elemental gold on the surface of damaged tissue was verified by electron probe microanalysis using energy dispersive spectroscopy. Note that the crack along the entire length of each scratch in electron micrographs occurred upon drying the specimen for electron microscopy and was therefore not labeled by functionalized Au NPs.

Further evidence for targeted labeling was provided by control groups and control specimens. As-synthesized (non-functionalized) Au NPs exhibited no apparent labeling of damaged tissue relative to undamaged tissue (not shown). Moreover, surface roughness control specimens also exhibited low levels of labeling in both damaged and undamaged regions of tissue (not shown) comparable to undamaged regions in experimental groups (Fig. 4). These observations suggest that targeted labeling of damaged tissue by functionalized Au NPs was due to the calcium specificity of the molecular groups and not due to an electrostatic association or increased surface roughness of the damaged tissue. Thus, both visual observation and backscattered electron microscopy provided qualitative evidence for targeted labeling of damaged tissue by functionalized Au NPs and suggested that bisphosphonate-functionalized Au NPs provided the greatest binding affinity (Fig. 4), consistent with previous experiments for binding to synthetic hydroxyapatite crystals (Ross and Roeder 2011).

Au NPs were directly observed as nanoscale spheres labeling damaged tissue surfaces at higher magnification using FE-SEM (Fig. 5). Similar features were not observed on the surface of the imaging control specimens in the absence of Au NPs (Fig. 5). The measured surface density of functionalized Au NPs was significantly greater on damaged tissue inside the scratch compared to undamaged tissue outside the

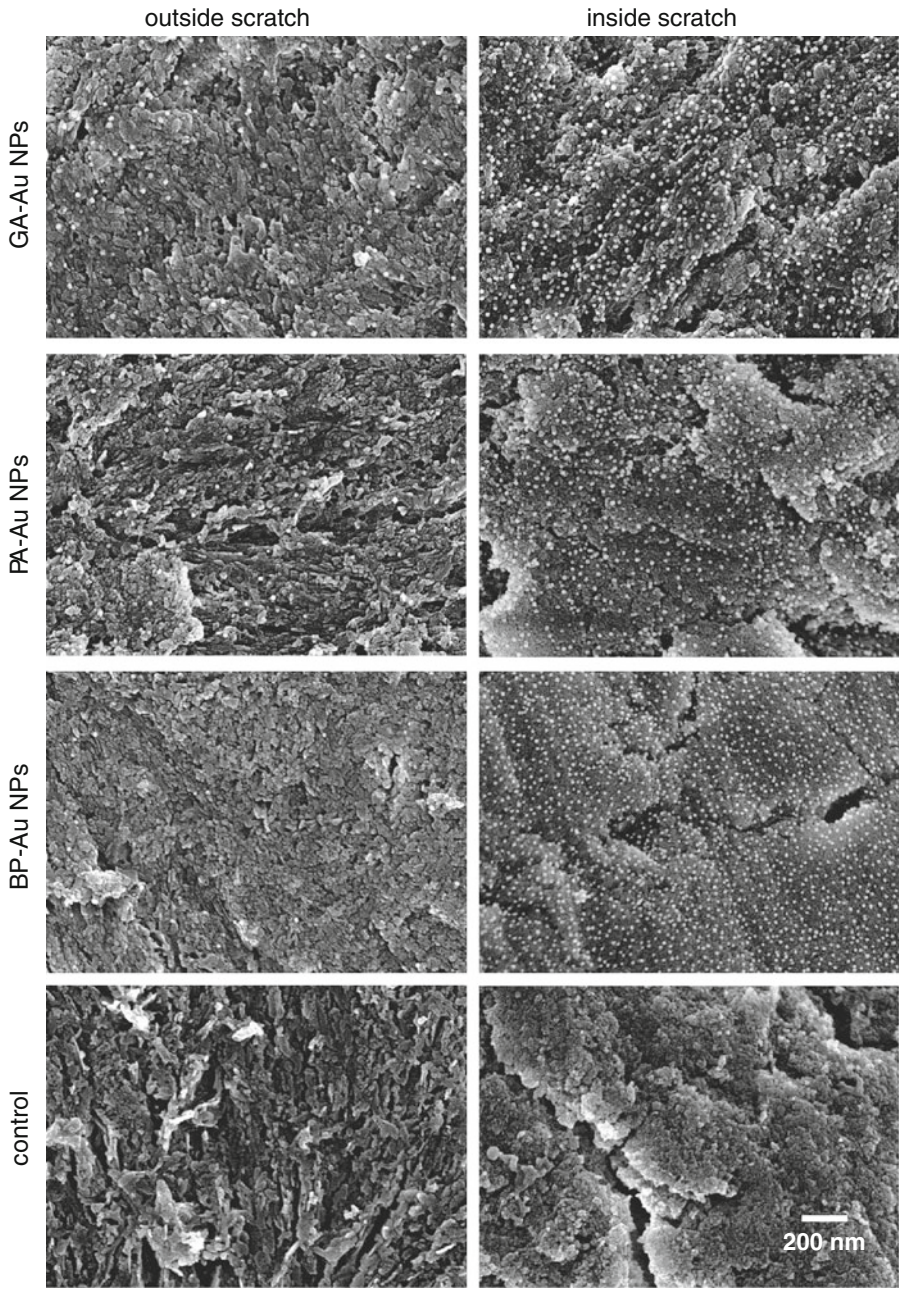

Fig. 5 Representative high magnification FE-SEM micrographs showing the surface density of glutamic acid (GA)-, phosphonic acid (PA)-, and bisphosphonate (BP)-functionalized Au NPs labeling damaged bone tissue inside the scratch versus undamaged tissue outside the scratch. The surface density of Au NPs was noticeably greater within damaged tissue, indicating targeted labeling. A control specimen that was scratched but not labeled verified that the observed spherical nanoparticles were not due to the inherent structure of the tissue

scratch for each functional group ($p < 0.05$, Tukey's HSD) (Fig. 6). Bisphosphonate-functionalized Au NPs exhibited a greater surface density labeling damaged tissue compared to glutamic acid- and phosphonic acid-functionalized Au NPs ($p < 0.05$, Tukey's HSD) (Fig. 6). In contrast, the surface density of Au NPs labeling of undamaged tissue outside the scratch was independent of the functional group (Fig. 6).

Control specimens again verified that the significantly greater surface density of Au NPs labeling damaged tissue inside the scratch compared to undamaged tissue outside the scratch for each functional group (Fig. 6) was due to targeted labeling. Surface roughness control specimens exhibited no difference in the surface density of bisphosphonate-functionalized Au NP labeling of damaged tissue

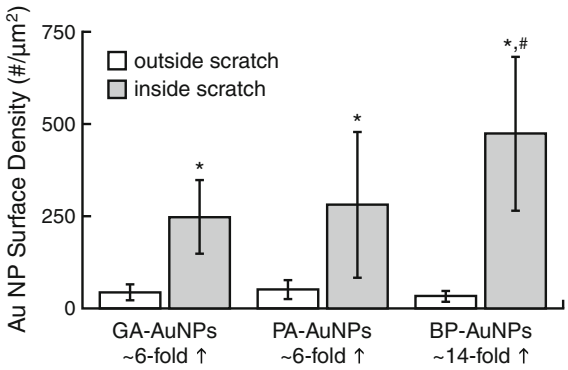

Fig. 6 The mean (±standard deviation) surface density of glutamic acid (GA)-, phosphonic acid (PA)-, and bisphosphonate (BP)-functionalized Au NPs labeling damaged bone tissue inside the scratch versus undamaged tissue outside the scratch. The Au NP surface density was significantly greater on damaged bone tissue inside the scratch compared undamaged tissue outside the scratch for each functional group ($^{*}p < 0.05$, Tukey's HSD). The Au NP surface density labeling damaged tissue was significantly greater for BP-Au NPs compared to GA-Au NPs and PA-Au NPs ($^{\#}p < 0.05$, Tukey's HSD)

inside the scratch (36.7 μm^{-2}) compared to undamaged tissue outside the scratch for either the control specimens (37.3 μm^{-2}) or the experimental groups (Fig. 6). These relatively constant levels were indicative of competitive adsorption between calcein and functionalized Au NPs. Calcein staining blocked the calcium-binding sites exposed by either specimen machining or the scratch, requiring functionalized Au NPs to displace calcein molecules. The surface roughness control specimens also demonstrated that differences between the surface density of functionalized Au NPs labeling damaged tissue inside the scratch versus undamaged tissue outside scratch (Fig. 6) were not due to the greater surface area available in the scratched tissue. Therefore, these results provided quantitative evidence of targeted labeling due to the calcium affinity of the functional groups, further supporting qualitative observations from visual observation and backscattered electron microscopy (Fig. 4).

The greater surface density of bisphosphonate-functionalized Au NPs labeling damaged tissue compared to glutamic acid- and phosphonic acid-functionalized Au NPs (Figs. 5, 6) was consistent with a previous report comparing the binding affinity of the same functionalized Au NPs to hydroxyapatite crystals (Ross and Roeder 2011). Thus, targeted labeling and the greater binding affinity of bisphosphonate-functionalized Au NPs were not affected by the presence of organic matter or differences in biological apatite versus synthetic hydroxyapatite crystals. Moreover, bisphosphonate-functionalized Au NPs exhibited a greater binding affinity to damaged tissue compared to glutamic acid- and phosphonic acid-functionalized Au NPs despite the fact that the surface density of bisphosphonate on Au NPs was previously measured to be ~50 % lower than glutamic acid and phosphonic acid, due to the greater size of the bisphosphonate molecules (Ross and Roeder 2011). The stability constant for bisphosphonate binding to bone mineral would be expected to be greater than for phosphonic acid due to the formation of bidentate, and possibly even tridentate (Nancollas et al. 2006), versus monodentate ligands, respectively. Bidentate chelation of calcium would also be expected for glutamic acid, but the greater acidity phosphonate groups compared to carboxylate groups is most likely responsible for the greater binding affinity of bisphosphonate.

A direct comparison between the binding affinity of functionalized Au NPs to bone tissue versus synthetic hydroxyapatite crystals is difficult due to differences in the binding substrates. Nonetheless, the binding affinity (surface density) of the functionalized Au NPs to bone tissue in this study was more than one order of magnitude lower than previous measurements for synthetic hydroxyapatite crystals (Ross and Roeder 2011), confirming the increased heterogeneity and decreased number of calcium-binding sites in damaged tissue samples compared to synthetic hydroxyapatite crystals.

The Au NP surface density was measured based on the projected surface area but surfaces clearly exhibited a nanotopography (Fig. 5). Therefore, measurements of the true surface area accounting for topography would decrease the measured Au NP surface density, but would not be expected to change the relative differences measured either inside versus outside the scratch, or between experimental groups (Fig. 6). The effects of random variation in surface roughness was mitigated by performing measurements on three fields of view per specimen for five specimens per group. Furthermore, the surface roughness control specimens demonstrated that differences in surface roughness inside versus outside the scratch had no measureable effect on the surface density of Au NPs.

Scratched tissue specimens were used as an experimental model to investigate labeling of damaged bone

tissue in several previous studies (O'Brien et al. 2002; Lee et al. 2003; Parkesh et al. 2007; Zhang et al. 2010). The creation of surface damage exposes mineral crystals, and therefore calcium-binding sites, otherwise surrounded by collagen and coated with noncollagenous proteins. The calcium-binding sites act as a target for the anionic molecular functional groups on the Au NPs. Calcein labeling chelated and therefore masked calcium-binding sites formed as a result of specimen machining or the scratch itself in surface roughness control specimens. This model facilitated the creation of controlled regions of damage adjacent to undamaged tissue on specimen surfaces which were readily imaged by optical and electron microscopy. A limitation of the model is that it did not allow investigation of delivery into tissue specimens, which should be the subject of further investigation both in vitro and in vivo. However, the vascular stability and half-life of functionalized Au NPs (Hainfeld et al. 2006; Cai et al. 2007; Kim et al. 2007), combined with strain-induced fluid flow within bone tissue (Knothe-Tate et al. 2000), are expected to promote delivery to damaged bone tissue in vivo.

Another possible limitation of this study was that experiments for targeted labeling of damaged bone tissue were carried out in water and not PBS or FBS. The rationale was that while PBS and FBS would certainly result in a lower relative binding affinity compared to water, targeted labeling would still occur and relative differences in binding affinity would be preserved between Au NPs with different functional groups (Ross and Roeder 2011). Moreover, functionalized Au NPs were shown to maintain colloidal stability in PBS and FBS and can therefore be reasonably expected to maintain colloidal stability during targeted delivery in vivo. In summary, the results of this study for targeted labeling of damaged bone tissue and colloidal stability in physiological media in vitro provide motivation for future in vivo investigation.

Conclusions

Au NPs surface-functionalized with either carboxylate (L-glutamic acid), phosphonate (2-aminoethylphosphonic acid), or bisphosphonate (alendronate) were shown to exhibit targeted labeling of damaged bone tissue in vitro. Bisphosphonate-functionalized Au NPs exhibited a greater binding affinity to damaged bone tissue compared to glutamic acid- and phosphonic acid-functionalized Au NPs, consistent with previous measurements for binding to synthetic hydroxyapatite crystals. Targeted labeling was enabled not only by the molecular functional groups but also by the colloidal stability in solution. Functionalized Au NPs were stabilized by the presence of the functional groups, and were shown to remain well dispersed in ionic (PBS) and serum (FBS) solutions for up to 1 week. Therefore, the results of this study suggest that bisphosphonate-functionalized Au NPs have potential for targeted delivery to damaged bone tissue in vitro and provide motivation for in vivo investigation.

Acknowledgments This research was supported by the U.S. Army Medical Research and Materiel Command (W81XWH-06-1-0196) through the Peer Reviewed Medical Research Program (PR054672). The authors acknowledge the Notre Dame Integrated Imaging Facility (NDIIF) and Tatyana Orlova for assistance with the FE-SEM.

References

Alkilany AM, Nagaria PK, Hexel CR, Shaw TJ, Murphy CJ, Wyatt MD (2009) Cellular uptake and cytotoxicity of gold nanorods: molecular origin of cytotoxicity and surface effects. Small 5(6):701–708

Aslam M, Fu L, Su M, Vijayamohanan K, Dravid VP (2004) Novel one-step synthesis of amine-stabilized aqueous colloidal gold nanoparticles. J Mater Chem 14:1795–1797

Burr DB, Forwood MR, Fyhrie DP, Martin RB, Schaffler MB, Turner CH (1997) Bone microdamage and skeletal fragility in osteoporotic and stress fractures. J Bone Miner Res 12(1):6–15

Cai QY, Kim SH, Choi KS, Kim SY, Byun SJ, Kim KW, Park SH, Juhng SK, Yoon K-H (2007) Colloidal gold nanoparticles as a blood-pool contrast agent for X-ray computed tomography in mice. Invest Radiol 42(12):797–806

Chapurlat BD, Delmas PD (2009) Bone microdamage: a clinical perspective. Osteoporos Int 20:1299–1308

Eck W, Nicholson AI, Zentgraf H, Semmler W, Bartling S (2010) Anti-CD4-targeted gold nanoparticles induce specific contrast enhancement of peripheral lymph nodes in X-ray computed tomography of lice mice. Nano Lett 10(7):2318–2322

Hainfeld JF, Slatkin DN, Focella TM, Smilowitz HM (2006) Gold nanoparticles: a new X-ray contrast agent. Br J Radiol 79(939):248–253

Hainfeld JF, O'Connor MJ, Bilmanian FA, Slatkin DN, Adams DJ, Smilowitz HM (2010) Micro-CT enables microlocalisation and quantification of Her2-targeted gold nanoparticles within tumour regions. Br J Radiol 84(1002):526–533

Hermann R, Walther P, Muller M (1996) Immunogold labeling in scanning electron microscopy. Histochem Cell Biol 106:31–39

Jackson PA, Rahman WNWA, Wong CJ, Ackerly T, Geso M (2010) Potential dependent superiority of gold nanoparticles in comparison to iodinated contrast agents. Eur J Radiol 75(1):104–109

Kim D, Park S, Lee JH, Jeong YY, Jon S (2007) Antibiofouling polymer-coated gold nanoparticles as a contrast agent for in vivo X-ray computed tomography imaging. J Am Chem Soc 129(24):7661–7665

Knothe-Tate ML, Steck R, Forwood MR, Niederer P (2000) In vivo demonstration of load-induced fluid flow in the rat tibia and its potential implications for processes associated with functional adaptation. J Exp Biol 203:2737–2745

Kumar A, Mandal S, Selvakannan PR, Pasricha R, Mandale AB, Sastry M (2003) Investigation into the interaction between surface-bound alkylamines and gold nanoparticles. Langmuir 19:6277–6282

Landrigan MD, Li J, Turnbull TL, Burr DB, Niebur GL, Roeder RK (2011) Contrast-enhanced micro-computed tomography of fatigue microdamage accumulation in human cortical bone. Bone 48(3):443–450

Lee TC, Mohsin S, Taylor D, Parkesh R, Gunnlaugsson T, O'Brien FJ, Giehl M, Gowin W (2003) Detecting microdamage in bone. J Anat 203:161–172

Leff DV, Brandt L, Heath JR (1996) Synthesis and characterization of hydrophobic, organically-soluble gold nanocrystals functionalized with primary amines. Langmuir 12:4723–4730

Leng H, Wang X, Ross RD, Niebur GL, Roeder RK (2008) Micro-computed tomography of fatigue microdamage in cortical bone using a barium sulfate contrast agent. J Mech Behav Biomed Mater 1(1):68–75

Nancollas GH, Tang R, Phipps RJ, Henneman Z, Gulde S, Wu W, Mangood A, Russell RGG, Ebetino FH (2006) Novel insights into actions of bisphosphonates on bone: differences in interactions with hydroxyapatite. Bone 38:617–627

O'Brien FJ, Taylor D, Lee TC (2002) An improved labelling technique for monitoring microcrack growth in compact bone. J Biomech 35:523–526

Parkesh R, Mohsin S, Lee TC, Gunnlaugsson T (2007) Histological, spectroscopic, and surface analysis of microdamage in bone: toward real-time analysis fluorescent sensors. Chem Mater 19:1656–1663

Podzimek S (2011) Light scattering, size exclusion chromatograph and asymmetric field flow fractionation. Wiley, Hoboken

Popovtzer R, Agrawal A, Kotov NA, Popovtzer A, Balter J, Carey TE, Kopelman R (2008) Targeted gold nanoparticle enable molecular CT imaging of cancer. Nano Lett 8(12):4593–4596

Ross RD, Roeder RK (2011) Binding affinity of surface functionalized gold nanoparticles for hydroxyapatite. J Biomed Mater Res 99A:58–66

Selvakannan PR, Mandal S, Phadtare S, Pasricha R, Sastry M (2003) Capping of gold nanoparticles by the amino acid lysine renders them water-dispersible. Langmuir 19:3545–3549

Sperling RA, Gil PR, Zhang F, Zanella M, Parak WJ (2008) Biological applications of gold nanoparticles. Chem Soc Rev 37:1896–1908

Stirling JW (1990) Immuno- and affinity probes for electron microscopy: a review of labeling and preparation techniques. J Histochem Cytochem 38:145–157

Turkevich J, Stevenson PC, Hillier J (1951) Synthesis of colloidal gold. Discuss Faraday Soc 11:55–75

Turnbull TL, Gargac JA, Niebur GL, Roeder RK (2011) Detection of fatigue microdamage in whole rat femora using contrast-enhanced micro-computed tomography. J Biomech 44:2395–2400

Wang X, Masse DB, Leng H, Hess KP, Ross RD, Roeder RK, Niebur GL (2007) Detection of trabecular bone microdamage by micro-computed tomography. Biomechanics 40(15):3397–3403

Xu C, Tung GA, Sun S (2008) Size and concentration effect of gold nanoparticles on X-ray attenuation as measured on computed tomography. Chem Mater 20(13):4167–4169

Zhang Z, Ross RD, Roeder RK (2010) Preparation of functionalized gold nanoparticles as a targeted X-ray contrast agent for damaged bone tissue. Nanoscale 2(4):582–586